# Spectra and energy levels of $Gd^{3+}(4f^7)$ in AlN

John B. Gruber*
*Department of Physics, San José State University, San José, California 95192-0106, USA*

Ulrich Vetter and Hans Hofsäss
*2. Physikalisches Institut, Universität Göttingen, Bunsenstr. 7-9, D-37073 Göttingen, Germany*

Bahram Zandi
*ARL/Adelphi Laboratory Center, US Army, Adelphi, Maryland 20783-1197, USA*

Michael F. Reid
*Department of Physics and Astronomy, University of Canterbury, Christchurch, New Zealand*
(Received 29 December 2003; published 19 May 2004)

We report crystal-field splitting investigations of $Gd^{3+}(4f^7)$ energy levels determined from high resolution energy (Stark) level cathodoluminescence (CL) spectroscopy of Gd-implanted 2H-aluminum nitride (AlN) in the wavelength range 250 to 320 nm and at temperatures 12, 77, and 300 K. The CL spectra are interpreted in terms of lattice-sum and crystal-field splitting models that assume implanted Gd replaces Al substitutionally in cationic sites in AlN having $C_{3v}$ point group symmetry. The CL spectra are associated with $Gd^{3+}$ ions in a single site. A rms deviation of 7 $cm^{-1}$ was obtained between 43 observed and calculated Stark levels. The intense UV emission at 318 nm (the $^6P_{7/2} \rightarrow {}^8S_{7/2}$ transition) can be understood in terms of multiplet-to-multiplet branching ratios.

DOI: 10.1103/PhysRevB.69.195202 PACS number(s): 78.60.Hk, 78.40.Fy, 71.70.Ch

## I. INTRODUCTION

Wide band gap semiconductors have considerable potential as components in optoelectronic devices, especially when implanted with trivalent rare earth (RE) ions.[1–9] Optically characterized by intra-$4f$ electronic transitions, these ions emit electromagnetic radiation at discrete wavelengths ranging from the ultraviolet (UV) to the infrared (IR).[10–14] As phosphor illuminators, these materials play an important role in the design of white light emitters.[15,16]

Because of its material and optical properties, 2H-aluminum nitride[17] (AlN) has been investigated as a host for light emitters implanted with $Er^{3+}$, $Eu^{3+}$, $Tb^{3+}$, and recently, $Gd^{3+}$ and $Tm^{3+}$ as a blue and UV light emitter.[1–9,18] AlN has a high thermal conductivity and stability; it is chemically inert in most environments, and has a band gap of more than 6 eV (50 000 $cm^{-1}$).[17] Such a wide band gap allows for UV emission from RE ion levels that are otherwise unavailable in *w*-GaN or 6H-SiC having band gaps less than 30 000 $cm^{-1}$.[17] Even many insulator crystal hosts exhibit strong lattice absorption above 35 000 $cm^{-1}$.[11]

In addition to device applications, AlN as a host for RE ions allows for possible detailed investigations of the crystal-field splitting of high-energy $4f^n$ states, $4f^{n-1}5d$ states, and the determination of free-ion parameters of lanthanide configurations, $4f$,[6–8] whose values are poorly known due to the lack of sufficient experimental energy (Stark) level data.[14] Also closer scrutiny is possible concerning the basic premise that forbidden electric-dipole transitions within the $4f^n$ configuration are due to mixing of states of opposite parity through the odd terms in the crystal-field expansion about the cationic site in the host lattice.[12,19,20]

Recent crystal-field splitting analyses of lanthanide-doped GaN[21–23] based on luminescence data for $Pr^{3+}$, $Sm^{3+}$, and $Tb^{3+}$ suggest that similar studies can be performed successfully as well on RE ion-doped AlN, and in particular on $Gd^{3+}$ and $Tm^{3+}$-doped AlN, where the size of the band gap permits direct observations of luminescence from the sextet states of $Gd^{3+}(4f^7)$ and the $^3P_J$, $^1I_6$ states of $Tm^{3+}(4f^{12})$.[9,24]

In the present study, the interpretation of the $Gd^{3+}$ cathodoluminescence (CL) spectra that we report, and the $Tm^{3+}$ (CL) spectra, which will appear in a subsequent presentation, are consistant with results obtained from lattice-sums calculations and crystal-field splitting modeling that assumes that the implanted $Gd^{3+}$ and $Tm^{3+}$ ions in AlN take substitutional Al lattice sites of $C_{3v}$ symmetry. That there appears to be no change in the local cationic symmetry between implanted $Gd^{3+}$ and $Tm^{3+}$ ions is contrary to what has been found between $Sm^{3+}$, $Tb^{3+}$, and $Er^{3+}$ in GaN, where the change from $C_{3v}$ symmetry for $Sm^{3+}$ in GaN to $D_2$ symmetry in $Tb^{3+}$ and $Er^{3+}$ in GaN is postulated as due to local structural changes based on differences in RE ionic radii.[23]

While the outcome of the crystal-field modeling is to establish consistency between calculated and experimental $^{2S+1}L_J$ multiplet manifold splittings, an important input parameter for lattice-sum calculations is the lattice location of the RE ions, or, in other words, the position and symmetry of the ion in the unit cell. An attractive direct determination of the ion's lattice location is provided by the emission channeling (EC) technique,[25] which uses charged particles emitted in the decay of radioactive ions for lattice location studies. Nearly all lanthanides have a satisfactory decay chain that has made EC studies successful in determining lattice locations in semiconductors like, e.g., Si, InP, GaAs, SiC,

 

GaN, diamond, *c*-BN and AlN.[8,9,26–30] Recently, in carrying out lattice location studies for $Yb^{3+}$ in AlN,[9] we showed that RE ions implanted into AlN take substitutional Al lattice sites for annealing temperatures in the range 293 K to 1273 K. This position within the AlN unit cell has $C_{3v}$ symmetry and represents the starting point for our lattice sum calculations.[31–33] Included in the present investigations are the details of the observed crystal-field splitting of the energy levels of $Gd^{3+}$ in AlN as obtained from an analysis of the observed cathodoluminescence spectra obtained at 12 K, 77 K, and 300 K. Intensities are reported in arbitrary units at different temperatures and show the relatively intense emission between the first excited manifold and the ground state ($^6P_{7/2} \rightarrow {}^8S_{7/2}$), which makes $Gd^{3+}$ the ion of choice for implementing quantum cutting devices.[34,35] With modest adjustment to the crystal-field splitting parameters, $B_{nm}$, obtained from lattice-sum calculations, an rms deviation of 7 $cm^{-1}$ is obtained between 43 calculated-to-observed Stark levels.

## II. SAMPLE PREPARATION AND LUMINESCENCE MEASUREMENTS

Films of AlN, grown on substrates of 6H-SiC (0001) by metal-organic chemical vapor deposition (MOCVD), were obtained from commercial sources. Upon receipt, the substrate was cut into small pieces, rinsed in acetone and deionized water, and dried under a flow of nitrogen gas. Rutherford backscattering spectroscopy (RBS) revealed a film thickness of 200 nm. $^{158}$Gd ions were implanted into these films at energies of 100 keV and fluences of $3\times10^{13}$ ions/$cm^2$. Both RBS measurements and implantation techniques are described elsewhere.[36] During implantation, samples were tilted 10° to the incident beam to avoid channeling by the incident ions. The mean implantation depth was calculated to be $33\pm7$ nm, assuming an AlN film density of 3.23 g/$cm^3$.[37] Post-implantation annealing was carried out in a vacuum tube furnace at pressures near $10^{-6}$ mbar and at a temperature of about 1373 K for 30 min. Further details can be found in Ronning *et al.*[38]

For CL fluorescence measurements, implanted samples were mounted on the head of a closed-cycle helium refrigerator located inside the vacuum chamber. An electrically controller resistive heater placed at the refrigerator head allows one to adjust the sample temperatures between 12 K and 300 K. The excitation source consisted of a SPECS EQ22 Auger electron gun that provides electrons with energies in the range between 100 eV to 5 keV and beam currents between 0.01 $\mu$A and 150 $\mu$A.

Sample luminescence was passed through a quartz window and collected with a UV-coated achromate lens pair, before reaching the entrance slit of a Czerny-Turner-spectrograph, model Jobin-Yvon 1000M. The light was dispersed using a holographic grating, blazed at 300 nm, with 1200 lines/mm, and detected by a nitrogen-cooled CCD camera, model Jobin-Yvon, UV-enhanced CCD (EEV CCD30-11). Exposure times for the spectra ranged from 1 s to 180 s. Unavoidable cosmic spikes that occur during long exposure times were identified by measuring each of the spectra at least twice and were manually removed from the experimental data. The spectrograph was repeatedly calibrated using the air wavelengths of spectral lines from a mercury lamp standard.[39] The uncertainty in wavelength measurements was about 0.02 nm. Temperature-dependent measurements were made on transitions at a given wavelength without moving the grating or otherwise disturbing the experimental setup in order to minimize inaccuracies in the measurements.

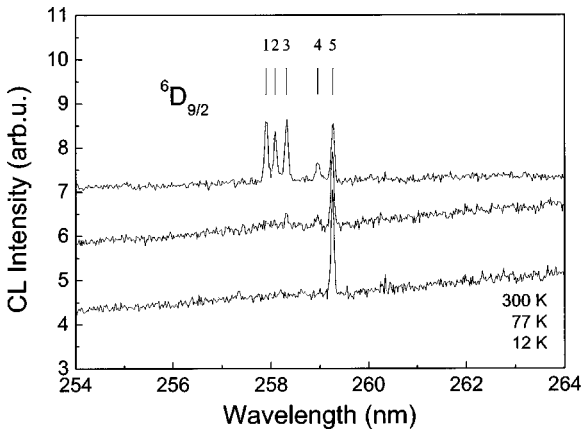


FIG. 1. CL spectra of the $^6D_{9/2} \rightarrow {}^8S_{7/2}$ transition of $Gd^{3+}$ in AlN, recorded between 254 and 264 nm at 12, 77, and 300 K.

## III. OBSERVED LUMINESCENCE SPECTRA

Figures 1–4 present the CL spectra of the $^6D_J$, $^6I_J$, and $^6P_J$ states of $Gd^{3+}(4f^7)$ observed between 250 nm and 320 nm at temperatures of 12, 77, and 300 K, and under excitation conditions of 5 keV and 0.25 W/$cm^2$. With an increase in temperature, higher-energy Stark levels within a given multiplet manifold are populated so that at 300 K all expected $J+1/2$ Stark levels are observed for each Kramers manifold (see, for example, Fig. 1, the $^6D_{9/2}$ and Fig. 4, the $^6P_{5/2}$ and $^6P_{7/2}$ manifolds). The ground-state manifold, $^8S_{7/2}$, has such a small splitting (predicted to be less than 0.3 $cm^{-1}$) that its splitting is not observed in the present data.[10]

As we pointed out earlier in the analyses of the lumines-

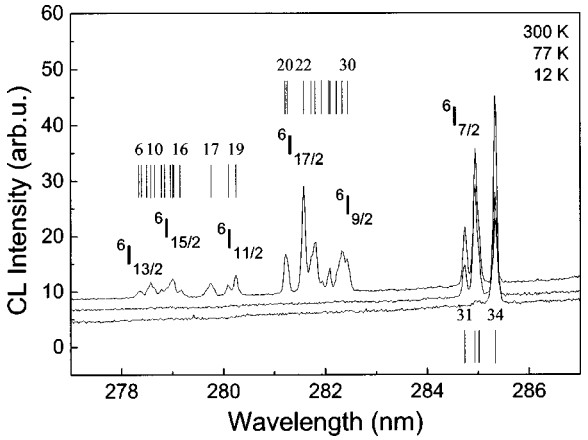


FIG. 2. CL spectra of the $^6I_{7/2,9/2,17/2,11/2,15/2,13/2} \rightarrow {}^8S_{7/2}$ transitions of $Gd^{3+}$ in AlN, recorded between 277 and 287 nm at 12, 77, and 300 K.

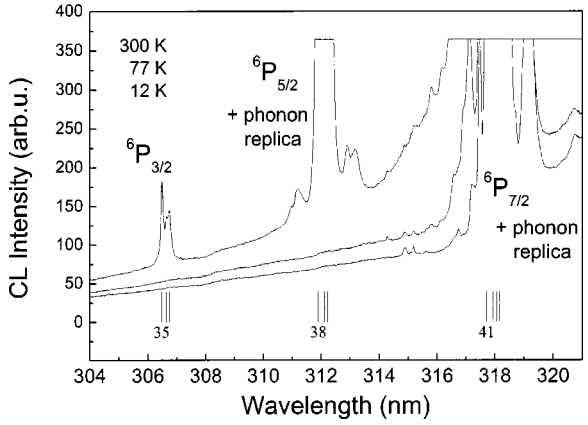


FIG. 3. CL spectra of the $^6P_{7/2,5/2,3/2} \rightarrow {}^8S_{7/2}$ transitions and phonon sidebands of $Gd^{3+}$ in AlN, recorded between 304 and 321 nm at 12, 77, and 300 K.

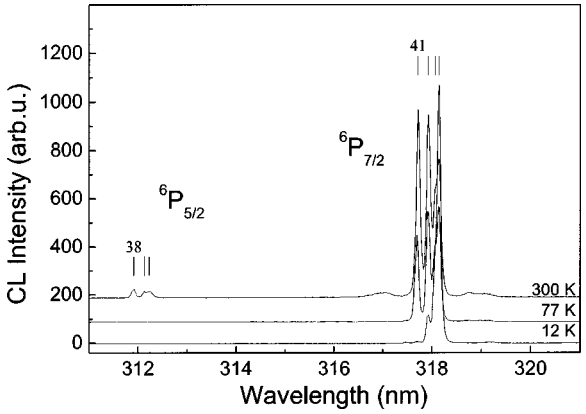


FIG. 4. CL spectra of the $^6P_{7/2,5/2} \rightarrow {}^8S_{7/2}$ transitions of $Gd^{3+}$ in AlN, recorded between 311 and 321 nm at 12, 77, and 300 K.

cence spectra of $Pr^{3+}$, $Sm^{3+}$, and $Tb^{3+}$ in GaN,[21–23] analyzing unpolarized CL spectra for transitions between individual Stark levels is primarily limited to matching repeated energy-level differences, similar to the technique used in analyzing the arc and spark spectra of ions and molecules for their energy-level configurations.[40] We are aided in the present study, however, by the number of $^{2S+1}L_J$ multiplet manifolds that are separated from one another by sufficient energy so that crystal-field mixing is minimal, and by the fact that the manifold splitting of the $^8S_{7/2}$ is so small that assignments for each level can be made with relative ease and are listed in Table I. For example, the splitting of the $^6D_{9/2}$ manifold (Fig. 1) is represented by transitions 1 through 5, and the splitting of the $^6P_{7/2}$ manifold (Fig. 4) is represented by transitions 41 through 44 in Table I, column 2. Both the size of the manifold splitting and the values of the energy levels ($cm^{-1}$) can be compared to similar data for $Gd^{3+}$ in fluoride, chloride, and oxide insulator host crystals with interesting results that support the nephelauxetic effect observed in rare earth systems.[10–13,41]

## IV. MODELING THE ENERGY LEVELS

A point-charge lattice-sum model described earlier[21–23] was adapted to analyze the crystal-field splitting of the $^{2S+1}L_J$ energy levels of $Gd^{3+}(4f^7)$ in AlN. From lattice location studies described by Vetter *et al.*[9] we conclude that implanted $Gd^{3+}$ in AlN take substitutional Al sites in the lattice that have $C_{3v}$ point group symmetry in a hexagonal structure with space group $C_{6v}^4 - P6_3$. The cell parameters are $a=b=3.11200$ Å, $c=4.99820$ Å, with $\alpha=\beta=90°$, and $\gamma=120°$. The lattice constants are similar to those for hexagonal GaN. The $c/a$ ratio is 1.601 for AlN and 1.625 for GaN.[42,43] Based on ionic radii and volume considerations, $Gd^{3+}$ should be accommodated in the Al sites.[42–45] The fact that $J+1/2$ transitions are identified in the spectra to each of the well isolated multiplet manifolds further indicates that $Gd^{3+}$ ions are found in a common site (see Figs. 1 and 4, for example). In AlN the axis of highest symmetry ($C_3$) is chosen as the $z$ axis (axis of quantization) and corresponds to the $c$ axis in the unit cell.[42]

The lattice-sum components $A_{nm}$, expressed in units of $cm^{-1}/Å^n$, are given as

$$A_{nm} = -e^2 \sum_j q_j \frac{C_{nm}(\hat{r}_j)}{r_j^{n+1}}, \tag{1}$$

where $q_j$ is the effective charge on the ion, and the sum is taken over all the ions in the lattice. By varying the formal charge of 3 on Al and N between 2.9 and 3.0 in our lattice-sum calculations, we find the assumption of isovalent impurity ($Gd^{3+}$) traps to be reasonable and consistent.[21,42–45]

The crystal-field splitting parameters $B_{nm}$, are related to the lattice-sum components by the expression $B_{nm}=\rho_n A_{nm}$ where the $\rho_n$ for $Gd^{3+}$ are $\rho_2=0.1668$, $\rho_4=0.4656$, and $\rho_6=1.1873$.[46] The $B_{nm}$ are in units of $cm^{-1}$ and the units of $\rho_n$ are $(Å^n)^{-1}$. The $B_{nm}$ parameters appear in the crystal-field Hamiltonian

$$H_{CF} = \sum_{n\ even} \sum_{m=-n}^{n} B_{nm}^* \sum_{i=1}^{N} C_{nm}(\hat{r}_i) \tag{2}$$

with the normalized one-electron tensor operators, $C_{nm}(\hat{r}_i)$, defined by[19]

$$C_{nm}(\hat{r}_i) = \sqrt{\frac{4\pi}{2n+1}} Y_{nm}(\theta_i, \phi_i) \tag{3}$$

and

$$C_{n,-m}(\hat{r}_i) = (-1)^m C_{nm}^*(r_i). \tag{4}$$

In Eq. (3), the $Y_{nm}$ are spherical harmonics, and $n=2$, 4 and 6 with $m=0$, $\pm 3$, and $\pm 6$, for $|m| \leqslant n$. The sum on $i$ in Eq. (2) runs over the seven $4f$ electrons (the half-filled shell) of $Gd^{3+}$.

The crystal field Hamiltonian given in Eq. (2) is diagonalized together with a parametrized free-ion Hamiltonian that includes coulombic, spin-orbit and interconfiguration interaction terms,

TABLE I. Energy levels of $Gd^{3+}$ $(4f^7)$ in AlN.[a]

| Level[b] $^{2S+1}L_J$ | No.[c] | λ[d] (nm) | $I$[e] (arb. units) | $E_{obs}$[f] ($cm^{-1}$) | $E_{calc}$[g] ($cm^{-1}$) | $\mu$[h] | Percent free-ion mixture |
|---|---|---|---|---|---|---|---|
| $^6P_{7/2}$ | 44 | 318.15 | 116.38\53.19\75.53 | 31423 | 31418 | ±1/2 | 99.7 $^6P_{7/2}$+0.07 $^6I_{13/2}$+0.07 $^6I_{15/2}$ |
| (31449) | 43 | 318.07 | 20.58\26.68\39.67 | 31431 | 31422 | ±1/2 | 99.7 $^6P_{7/2}$+0.08 $^6P_{5/2}$+0.07 $^6I_{17/2}$ |
| | 42 | 317.93 | 10.51\53.27\97.40 | 31444 | 31449 | ±3/2 | 99.8 $^6P_{7/2}$+0.05 $^6I_{17/2}$+0.03 $^6I_{11/2}$ |
| | 41 | 317.72 | 3.06\41.09\92.63 | 31465 | 31468 | ±1/2 | 99.8 $^6P_{7/2}$+0.06 $^6I_{15/2}$+0.03 $^6I_{13/2}$ |
| $^6P_{5/2}$ | 40 | 312.23 | -\-\6.99 | 32018 | 32020 | ±3/2 | 99.6 $^6P_{5/2}$+0.14 $^6I_{17/2}$+0.13 $^6I_{7/2}$ |
| (32043) | 39 | 312.13 | -\-\1.58 | 32029 | 32025 | ±1/2 | 99.7 $^6P_{5/2}$+0.09 $^6P_{7/2}$+0.08 $^6I_{17/2}$ |
| | 38 | 311.91 | -\-\5.3 | 32051 | 32050 | ±1/2 | 99.6 $^6P_{5/2}$+0.17 $^6I_{17/2}$+0.15 $^6I_{7/2}$ |
| $^6P_{3/2}$ | 37 | 306.73 | -\-\17.52 | 32593 | 32585 | ±1/2 | 99.6 $^6P_{3/2}$+0.14 $^6I_{15/2}$+0.09 $^6I_{9/2}$ |
| (32602) | 36 | 306.62 | -\-\4.77 | 32604 | 32596 | ±3/2 | 99.5 $^6P_{3/2}$+0.16 $^6I_{13/2}$+0.14 $^6I_{11/2}$ |
| | 35 | 306.47 | -\-\13.4 | 32620 | | | |
| $^6I_{7/2}$ | 34 | 285.34 | 4.98\2.47\1.49 | 35036 | 35040 | ±1/2 | 99.8 $^6I_{7/2}$+0.14 $^6I_{9/2}$+0.03 $^6P_{5/2}$ |
| (35076) | 33 | 285.02 | -\1.19\1.35 | 35075 | 35076 | ±1/2 | 99.6 $^6I_{7/2}$+0.27 $^6I_{9/2}$+0.05 $^6P_{5/2}$ |
| | 32 | 284.94 | -\2.18\2.71 | 35085 | 35079 | ±3/2 | 99.7 $^6I_{7/2}$+0.13 $^6I_{9/2}$+0.12 $^6P_{5/2}$ |
| | 31 | 284.74 | -\0.9–1.66 | 35109 | 35118 | ±1/2 | 99.8 $^6I_{7/2}$+0.11 $^6P_{5/2}$+0.02 $^6I_{9/2}$ |
| $^6I_{9/2}$ | 30 | 282.44 | | 35395 | 35380 | ±1/2 | 99.3 $^6I_{9/2}$+0.28 $^6I_{17/2}$+0.24 $^6I_{7/2}$ |
| (35420) | 29 | 282.33 | | 35409 | 35400 | ±1/2 | 98.7 $^6I_{9/2}$+0.78 $^6I_{17/2}$+0.25 $^6I_{11/2}$ |
| | 28 | 282.22 | | 35423 | 35414 | ±3/2 | 98.8 $^6I_{9/2}$+0.53 $^6I_{17/2}$+0.46 $^6I_{17/2}$ |
| | 27 | 282.09 | | 35439 | 35453 | ±3/2 | 98.3 $^6I_{9/2}$+1.15 $^6I_{17/2}$+0.20 $^6I_{11/2}$ |
| | 26 | 282.06 | | 35443 | 35458 | ±1/2 | 96.7 $^6I_{9/2}$+2.86 $^6I_{17/2}$+0.20 $^6I_{11/2}$ |
| $^6I_{17/2}$ | 25 | 281.92 | | 35461 | 35475 | ±1/2 | 99.5 $^6I_{17/2}$+0.22 $^6I_{13/2}$+0.14 $^6I_{15/2}$ |
| (35479) | | | | | 35476 | ±3/2 | 98.4 $^6I_{17/2}$+0.75 $^6I_{9/2}$+0.64 $^6I_{15/2}$ |
| | 24 | 281.80 | | 35476 | 35477 | ±1/2 | 98.5 $^6I_{17/2}$+0.66 $^6I_{9/2}$+0.43 $^6I_{15/2}$ |
| | | | | | 35478 | ±1/2 | 98.2 $^6I_{17/2}$+0.28 $^6I_{9/2}$+0.20 $^6I_{11/2}$ |
| | | | | | 35480 | ±3/2 | 98.8 $^6I_{17/2}$+0.69 $^6I_{9/2}$+0.33 $^6I_{11/2}$ |
| | 23 | 281.72 | | 35486 | 35483 | ±1/2 | 98.5 $^6I_{17/2}$+0.20 $^6I_{13/2}$+0.13 $^6I_{9/2}$ |
| | 22 | 281.57 | | 35505 | 35495 | ±1/2 | 98.4 $^6I_{17/2}$+1.03 $^6I_{9/2}$+0.21 $^6I_{15/2}$ |
| | 21 | 281.25 | | 35535 | 35540 | ±3/2 | 99.1 $^6I_{17/2}$+0.22 $^6I_{15/2}$+0.18 $^6I_{11/2}$ |
| | 20 | 281.21 | | 35550 | 35550 | ±1/2 | 97.5 $^6I_{17/2}$+1.79 $^6I_{9/2}$+0.26 $^6I_{13/2}$ |
| $^6I_{11/2}$ | 19 | 280.24 | | 35673 | 35670 | ±3/2 | 98.1 $^6I_{11/2}$+1.00 $^6I_{15/2}$+0.55 $^6I_{9/2}$ |
| (35711) | | | | | 35675 | ±1/2 | 98.8 $^6I_{11/2}$+0.56 $^6I_{15/2}$+0.18 $^6I_{17/2}$ |
| | 18 | 280.09 | | 35692 | 35694 | ±1/2 | 98.9 $^6I_{11/2}$+0.64 $^6I_{13/2}$+0.15 $^6I_{15/2}$ |
| | | | | | 35738 | ±1/2 | 95.6 $^6I_{11/2}$+2.61 $^6I_{15/2}$+1.32 $^6I_{13/2}$ |
| | 17 | 279.75 | | 35736 | 35739 | ±3/2 | 97.8 $^6I_{11/2}$+1.08 $^6I_{15/2}$+0.40 $^6I_{13/2}$ |
| | | 279.6 | | 35754 | 35750 | ±1/2 | 97.7 $^6I_{11/2}$+1.70 $^6I_{15/2}$+0.28 $^6I_{17/2}$ |
| $^6I_{15/2}$ | 16 | 279.14 | | 35814 | 35814 | ±1/2 | 96.1 $^6I_{15/2}$+3.40 $^6I_{11/2}$+0.28 $^6I_{17/2}$ |
| (35850) | | | | | 35819 | ±1/2 | 98.4 $^6I_{15/2}$+0.82 $^6I_{13/2}$+0.43 $^6I_{17/2}$ |
| $^6I_{13/2}$ | | | | | 35820 | ±3/2 | 80.2 $^6I_{15/2}$+18.4 $^6I_{13/2}$+0.63 $^6I_{11/2}$ |
| (35869) | 15 | 279.02 | | 35829 | 35827 | ±3/2 | 80.3 $^6I_{15/2}$+18.4 $^6I_{13/2}$+0.63 $^6I_{11/2}$ |
| | 14 | 279 | | 35832 | 35831 | ±1/2 | 95.3 $^6I_{13/2}$+3.16 $^6I_{15/2}$+1.25 $^6I_{17/2}$ |
| | 13 | 278.96 | | 35837 | 35841 | ±1/2 | 84.3 $^6I_{13/2}$+15.3 $^6I_{15/2}$+0.14 $^6I_{11/2}$ |
| | 12 | 278.84 | | 35852 | 35852 | ±1/2 | 85.2 $^6I_{15/2}$+14.3 $^6I_{13/2}$+0.26 $^6I_{11/2}$ |
| | 11 | 278.78 | | 35860 | 35865 | ±1/2 | 90.8 $^6I_{15/2}$+8.01 $^6I_{13/2}$+0.73 $^6I_{11/2}$ |
| | 10 | 278.65 | | 35877 | 35877 | ±3/2 | 97.5 $^6I_{15/2}$+1.35 $^6I_{13/2}$+0.73 $^6I_{11/2}$ |
| | | | | | 35881 | ±1/2 | 83.3 $^6I_{13/2}$+16.1 $^6I_{15/2}$+0.40 $^6I_{11/2}$ |
| | 9 | 278.57 | | 35887 | 35887 | ±3/2 | 98.5 $^6I_{15/2}$+0.64 $^6I_{13/2}$+0.56 $^6I_{11/2}$ |
| | | | | | 35890 | ±1/2 | 85.6 $^6I_{15/2}$+13.3 $^6I_{13/2}$+0.82 $^6I_{11/2}$ |
| | 8 | 278.49 | | 35897 | 35902 | ±3/2 | 97.9 $^6I_{13/2}$+1.35 $^6I_{15/2}$+0.36 $^6I_{11/2}$ |
| | 7 | 278.39 | | 35910 | 35904 | ±1/2 | 97.8 $^6I_{13/2}$+1.74 $^6I_{15/2}$+0.22 $^6I_{17/2}$ |
| | 6 | 278.34 | | 35917 | 35912 | ±1/2 | 98.9 $^6I_{13/2}$+0.71 $^6I_{15/2}$+0.16 $^6I_{17/2}$ |
| $^6D_{9/2}$ | 5 | 259.27 | -\-\0.11 | 38558 | 38573 | ±3/2 | 99.8 $^6D_{9/2}$+0.12 $^6D_{7/2}$+0.14 $^6I_{15/2}$ |
| (38671) | 4 | 258.96 | -\-\0.09 | 38604 | 38600 | ±1/2 | 99.7 $^6D_{9/2}$+0.14 $^6D_{7/2}$+0.04 $^6I_{15/2}$ |
| | 3 | 258.32 | -\-\0.12 | 38700 | 38692 | ±3/2 | 99.8 $^6D_{9/2}$+0.04 $^6D_{7/2}$+0.03 $^6I_{11/2}$ |

TABLE I. (*Continued.*)

| Level[b] $^{2S+1}L_J$ | No.[c] | λ[d] (nm) | $I$[e] (arb. units) | $E_{obs}$[f] ($cm^{-1}$) | $E_{calc}$[g] ($cm^{-1}$) | $\mu$[h] | Percent free-ion mixture |
|---|---|---|---|---|---|---|---|
| | 2 | 258.09 | -\-\0.09 | 38735 | 38729 | ±1/2 | 99.8 $^6D_{9/2}$+0.05 $^6D_{7/2}$+0.04 $^6I_{15/2}$ |
| | 1 | 257.90 | 0.19\0.13\0.12 | 38763 | 38762 | ±1/2 | 99.7 $^6D_{9/2}$+0.10 $^6D_{7/2}$+0.07 $^6D_{1/2}$ |
| $^6D_{1/2}$ | | | | | 39603 | ±1/2 | 83.9 $^6D_{1/2}$+15.7 $^6D_{7/2}$+0.25 $^6D_{5/2}$ |
| (39621) | | | | | | | |
| $^6D_{7/2}$ | | | | | 39679 | ±3/2 | 83.7 $^6D_{7/2}$+13.1 $^6D_{3/2}$+2.97 $^6D_{5/2}$ |
| (39713) | | | | | 39693 | ±1/2 | 87.8 $^6D_{7/2}$+11.0 $^6D_{3/2}$+0.94 $^6D_{5/2}$ |
| | | | | | 39721 | ±1/2 | 95.4 $^6D_{7/2}$+2.6 $^6D_{1/2}$+1.18 $^6D_{5/2}$ |
| | | | | | 39727 | ±1/2 | 85.2 $^6D_{7/2}$+12.8 $^6D_{1/2}$+1.14 $^6D_{3/2}$ |
| $^6D_{3/2}$ | | | | | 39847 | ±3/2 | 71.8 $^6D_{3/2}$+19.1 $^6D_{5/2}$+9.06 $^6D_{7/2}$ |
| (39851) | | | | | 39871 | ±1/2 | 74.5 $^6D_{3/2}$+15.6 $^6D_{5/2}$+9.63 $^6D_{7/2}$ |
| $^6D_{5/2}$ | | | | | 39952 | ±3/2 | 77.8 $^6D_{5/2}$+15.1 $^6D_{3/2}$+7.01 $^6D_{7/2}$ |
| (39978) | | | | | 39984 | ±1/2 | 83.4 $^6D_{5/2}$+12.4 $^6D_{3/2}$+3.96 $^6D_{7/2}$ |
| | | | | | 40062 | ±1/2 | 97.7 $^6D_{5/2}$+1.96 $^6D_{7/2}$+0.21 $^6D_{3/2}$ |

[a]Spectra obtained at 12, 77, and 300 K.

[b]$^{2S+1}L_J$ multiplet manifolds for $Gd^{3+}$ $(4f^7)$; the number in parenthesis indicates the calculated centroid for each manifold.

[c]Number of transition as assigned in the figures.

[d]Experimental wavelength in nanometers.

[e]CL intensity in arbitrary units at different temperatures $[I(12\,\mathrm{K})\backslash I(77\,\mathrm{K})\backslash I(300\,\mathrm{K})]$. Intensities of the $^6P_{7/2}\rightarrow{}^8S_{7/2}$ and $^6P_{5/2}\rightarrow{}^8S_{7/2}$ transitions have to be multiplied by ~50.

[f]Energy in vacuum wave numbers.

[g]Calculated splitting based on $Gd^{3+}$ in $C_{3v}$ sites: $B_{20}=-211$, $B_{40}=-1691$, $B_{43}=-1063$, $B_{60}=655.5$, $B_{63}=-188.4$, and $B_{66}=293.7$; rms 7 $cm^{-1}$, between 43 observed and calculated Stark levels.

[h]Symmetry label $\mu=\pm1/2$, $\mu=\pm3/2$, calculated using the $B_{nm}$ parameters in footnote g.

$$H_{FI}=H_0+E_{AVE}+\sum_{k=2,4,6} f_k F^k+\zeta\sum_{i=1}^{7}\mathbf{s}_i\cdot\mathbf{l}_i+\alpha L^2+\beta G(G_2)$$
$$+\gamma G(R_7)+\sum_{i=2,3,4,6,7,8} t_i T^i+\sum_{k=0,2,4} m_k M^k$$
$$+\sum_{k=2,4,6} p_k P^k, \qquad (5)$$

for the $4f^7$ electronic configuration, where the individual terms and definitions are detailed by Görller-Walrand and Binnemans,[47] and a starting set of free-ion parameters is given by Carnall *et al.*[48] for $Gd^{3+}$. These parameters are used to calculate the reduced matrix elements of $U^2$, $U^4$, and $U^6$ between all intermediate-coupled wavefunctions for the electronic configuration. A separate program takes the reduced matrix elements between the free-ion multiplets, sets up the crystal spaces for a given symmetry, and diagonalizes in that space of multiplets the crystal-field splitting Hamiltonian given in Eq. (2). The number of $^{2S+1}L_J$ free-ion eigenvectors is 327 for $4f^7$ with more than 2000 doubly-degenerate (Stark) energy eigenvalues spanning 180 000 $cm^{-1}$. A complete diagonalization of the energy matrix consisting of crystal quantum states $\mu=\pm1/2$ and $\mu=\pm3/2$ is not particularly useful given that only 19 $^{2S+1}L_J$ multiplets lie within the band gap, of which we have data for all but the $^6G_J$ multiplets. Instead, we diagonalize the complete Hamiltonian for the lowest-energy 25 multiplet manifolds, following the approach we used earlier to reduce truncation errors to a minimum.[49] Truncation errors are introduced when the *J*-mixing is large. In Table I the mixing is relatively small and suggests that the approximation made by truncation is reasonable for the levels observed in the CL spectra. In the following fitting scheme, we vary only the six $B_{nm}$, and the centroid for each multiplet in order to account for the relatively small crystal-field mixing between states. Fitting of the free ion parameters is not possible in our case, because for the observed free ion energy levels corresponding matrix elements are often too small, resulting in large uncertainties. Typical examples are the Slater parameters $F^k$. The starting set of $B_{nm}$ were obtained from lattice-sum calculations for GaN. With modest adjustment to the initial $B_{nm}$ parameters and centroids, we obtain final agreement between 43 experimental Stark levels and calculated levels with a rms deviation of 7 $cm^{-1}$. Based on the analysis of the observed spectra, the splitting of other multiplets, such as the $^6D_{1/2,7/2,3/2,5/2}$ are predicted and reported in Table I. The $^6G_J$ multiplets are predicted close to the band gap. Their multiplet splitting may be of interest for energy transfer between the conduction band and the ion, but we lack sufficient data at this time to determine the energy (Stark) levels for these multiplets.

## V. CATHODOLUMINESCENCE INTENSITIES

From Figs. 1–4 we obtain qualitative information concerning the emission characteristics that were first reported

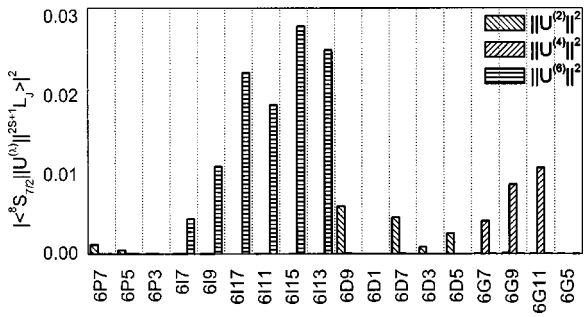


FIG. 5. Squared reduced matrix elements in units $cm^{-1}$ for transitions between ground state and first 18 excited $^{2S+1}L_J$ multiplet manifolds of $Gd^{3+}$ (notation $^{2S+1}L_{2J}$).

by Vetter *et al.*[24] for $Gd^{3+}$:AlN, particularly the intense emission identified from the four Stark levels of the $^6P_{7/2}$ to the ground state $^8S_{7/2}$ observed between 317.72 nm and 318.15 nm (transitions 41–45, Table I). There is a factor of 50 times greater intensity for these transitions as compared with all other transitions observed.

We can make a rough approximation of expected transition probabilities for electric- and magnetic-dipole transitions to the ground state using the parametrization methods developed by Axe,[50] and Krupke and Gruber,[51] which later evolved into the Judd-Ofelt approximation methods. The radiative transition probabilities are of the form[12,52]

$$W=\frac{64\pi^4e^2\langle\nu\rangle^3n(n^2+2)^2}{27h[J]}\times\sum_{\lambda=2,4,6}\Omega_\lambda|\langle^{2S+1}L_J\|U^{(\lambda)}\|^8S_{7/2}\rangle|^2\equiv\sum_{\lambda=2,4,6}A'^{(\lambda)}\Omega_\lambda, \tag{6}$$

where $n$ is the index of refraction at the wavelength of the transition, assuming an isotropic medium, $\langle\nu\rangle$ is the energy of the radiation in $cm^{-1}$, $|\langle\|U^{(\lambda)}\|\rangle|^2$ are the squared reduced matrix elements, and $\Omega_2$, $\Omega_4$, and $\Omega_6$ are the intensity parameters. For comparison, values of $\Omega_2$, $\Omega_4$, and $\Omega_6$ are reported by Sytsma *et al.*[53] based on analyses of emission data from $Gd^{3+}$ in other hosts.[41] The values of the squared reduced matrix elements for this study are given in Fig. 5 for manifold transitions between the ground state $^8S_{7/2}$, and excited $^6P_J$, $^6I_J$, $^6D_J$, and $^6G_J$ states.

In addition to radiative relaxations between $Gd^{3+}$ ion states, we need to consider nonradiative deexcitation due to multiphonon relaxation as well. The relatively small manifold splittings, and the closely spaced multiplets for many of the states reported in Table I, suggest that multiphonon relaxations will reduce the actual lifetime and observed emission from most states, with the possible exception of $^6D_{9/2}$, $^6I_{7/2}$, and $^6P_{7/2}$, the latter which is separated from the ground state by more than 31 000 $cm^{-1}$.

Since all emission from the $^6P_{7/2}$ goes directly to the ground state $^8S_{7/2}$, it is worthwhile to explore branching ratios from states higher in energy than $^6P_{7/2}$ to see if we can explain the intense emission observed at 318 nm reported by Vetter *et al.*[24] Since both even and odd crystal-field components $A_{nm}$ are obtained from lattice-sum calculations, and Stark levels and corresponding wave functions have been identified for $Gd^{3+}$ in AlN, we can model branching ratios following an approach outlined in our analysis of the CL spectra of $Sm^{3+}$ in GaN.[22]

Line-to-line branching ratios are computed as a function of temperature by including a partition function representing the population in individual Stark levels as

$$\beta_{ij}=\frac{z_iW_{ij}}{\Sigma_{ij}z_iW_{ij}}, \tag{7}$$

where

$$z_i=\frac{\exp(E_i/k_BT)}{\Sigma_i\exp(E_i/k_BT)}, \tag{8}$$

and $i$ represents the emitting Stark level. Multiplet branching ratios corresponding to the Judd-Ofelt method[53] are obtained by summing contributions from line-to-line transitions, each weighted equally ($z_i=1.0$ for all $i$). By calculating multiplet branching ratios from $^6G_{7/2}\rightarrow{}^6D_J$, $^6I_J$, $^6P_J$, $^8S_{7/2}$; $^6D_J\rightarrow{}^6I_J$, $^6P_J$, $^8S_{7/2}$; $^6I_J\rightarrow{}^6P_J$, $^8S_{7/2}$, we find substantial probability of decay to the $^6P_J$ states. Rapid relaxation among $^6P_J$ states leads to the prediction that the $^6P_{7/2}\rightarrow{}^8S_{7/2}$ transition at 318 nm is the most likely emission by several orders of magnitude. Based on analyses of the fluorescence spectra of $Gd^{3+}$ in other hosts and our modeling studies, we conclude that the $^6P_{7/2}\rightarrow{}^8S_{7/2}$ transition observed at 318 nm clearly dominates other radiative transitions possible between excited states not involving the ground state.

## VI. SUMMARY

In summary, we report a detailed crystal-field splitting analysis of $Gd^{3+}$ implanted in AlN. Lattice-sum calculations, and modeling of the crystal-field splitting supports our recent work indicating that the $Gd^{3+}$ ions substantially replace Al in lattice sites having $C_{3v}$ point group symmetry in hexagonal AlN. All the CL spectra are associated with $Gd^{3+}$ in a single site. Modest adjustments to six crystal field parameters $B_{nm}$, and to the centroid for each multiplet manifold, $^{2S+1}L_J$, leads to a rms deviation of 7 $cm^{-1}$ for 43 observed-to-calculated Stark levels. The intense UV emission at 318 nm (the $^6P_{7/2}\rightarrow{}^8S_{7/2}$ transition) can be understood in terms of multiplet-to-multiplet branching ratios based on a Judd-Ofelt analysis of the observed spectra.

*Electronic address: jbgruber@email.sjsu.edue

[1] H. Ennen and J. Schneider, J. Electron. Mater. **A14**, 115 (1985).
[2] S. Schmitt-Rink, C. Varma, and A. Levi, Phys. Rev. Lett. **66**, 2782 (1991).
[3] R. Wilson, R. Schwartz, C. Abernathy, S. Pearson, N. Newman, M. Rubin, T. Fu, and J. Zavada, Appl. Phys. Lett. **65**, 992 (1994).
[4] J. Zavada and D. Zhang, Solid-State Electron. **38**, 1285 (1995).
[5] A. Steckl and R. Birkhahn, Appl. Phys. Lett. **73**, 1700 (1998).
[6] X. Wu, U. Hömmerich, J. MacKenzie, C. Abernathy, S. Pearton, R. Wilson, R. Schwartz, and J. Zavada, J. Lumin. **72**, 284 (1997).
[7] K. Gurumurugan, M. Chen, G. Harp, W. Jadwisienczak, and H. Lozykowski, Appl. Phys. Lett. **74**, 3008 (1999).
[8] U. Vetter, T. Taniguchi, U. Wahl, J. Correia, A. Müller, C. Ronning, H. Hofsäss, M. Dietrich, and the ISOLDE Collaboration, in *Progress in Semiconductor Materials II—Electronic and Optoelectronic Applications*, edited by B. D. Weaver, M. O. Manasreh, C. Jagadish, and S. Zollner, MRS Symposia Proceedings No. 744 (Materials Research Society, Pittsburgh, 2003).
[9] U. Vetter, M. Reid, H. Hofsäss, C. Ronning, J. Zenneck, M. Dietrich, and the ISOLDE Collaboration, in *GaN and Related Alloys*, edited by E. T. Yu, Y. Arakawa, A. Rizzi, J. S. Speck, and C. M. Wetzel, MRS Symposia Proceedings No. 743 (Materials Research Society, Pittsburgh, 2003).
[10] G. Dieke, *Spectra and Energy Levels of Rare Earth Ions in Crystals* (Wiley-Interscience, New York, 1968).
[11] A. Kaminskii, *Laser Crystals* (Springer, New York, 1981).
[12] J. Gruber, *Optical Transitions in Rare Earth Crystals, Progress in Science and Technology of the Rare Earths* (Pergamon, London, 1968), Vol. 3.
[13] S. Hüfner, *Optical Spectra of Transparent Rare Earth Compounds* (Academic, New York, 1978).
[14] L. van Pieterson, M. Reid, R. Wegh, S. Soverna, and A. Meijerink, Phys. Rev. B **65**, 045113 (2002).
[15] C. Ronda, T. Jüstel, and H. Nikol, J. Alloys Compd. **275**, 669 (1998).
[16] J. Yum, S. Seo, S. Lee, and Y. Sung, J. Electrochem. Soc. **150**, H47 (2003).
[17] *Properties of Advanced Semiconductor Materials*, edited by M. Levinshtein, S. Rumyantsev, and M. Shur (Wiley, New York, 2001).
[18] W. Jadwisienczak, H. Lozykowski, I. Berishev, A. Bensaoula, and I. Brown, J. Appl. Phys. **89**, 4384 (2001).
[19] B. Judd, *Operator Techniques in Atomic Spectroscopy* (McGraw-Hill, New York, 1997).
[20] G. Ofelt, J. Chem. Phys. **37**, 511 (1962).
[21] J. Gruber, B. Zandi, H. Lozykowski, and W. Jadwisienczak, J. Appl. Phys. **89**, 7973 (2001).
[22] J. Gruber, B. Zandi, H. Lozykowski, and W. Jadwisienczak, J. Appl. Phys. **91**, 2929 (2002).
[23] J. Gruber, B. Zandi, H. Lozykowski, and W. Jadwisienczak, J. Appl. Phys. **92**, 5127 (2002).
[24] U. Vetter, J. Zenneck, and H. Hofsäss, Appl. Phys. Lett. **83**, 2145 (2003).
[25] H. Hofsäss and G. Lindner, Phys. Rep. **201**, 121 (1991).
[26] K. Bharuth-Ram, U. Vetter, H. Hofsäss, C. Ronning, and M. Dietrich, Nucl. Instrum. Methods Phys. Res. B **190**, 835 (2002).
[27] U. Wahl, A. Vantomme, G. Langouche, J. Araújo, L. Peralta, J. Correia, and the ISOLDE Collaboration, J. Appl. Phys. **88**, 1319 (2000).
[28] U. Wahl, A. Vantomme, J. De-Wachter, R. Moons, G. Langouche, J. Marques, J. Correia, and the ISOLDE Collaboration, Phys. Rev. Lett. **79**, 2069 (1997).
[29] U. Wahl, A. Vantomme, G. Langouche, and J. Araújo, Nucl. Instrum. Methods Phys. Res. B **175–177**, 262 (2001).
[30] U. Wahl, A. Vantomme, and G. Langouche, Nucl. Instrum. Methods Phys. Res. B **148**, 492 (1999).
[31] J. Gruber, *Modeling Spectroscopic Properties and Crystal-Field Effects in Wide Bandgap Semiconductors Doped with Rare Earths* (SPIE, Bellingham, WA, 2001).
[32] J. Gruber and B. Zandi, Proc. ICFE Fourth International Conference of f-Elements **421**, 13 (2000).
[33] C. Morrison, *Angular Momentum Theory Applied to Interaction in Solids* (Springer, New York, 1988).
[34] B. Liu, Y. Chen, C. Shi, H. Tang, and Y. Tao, J. Lumin. **101**, 155 (2003).
[35] R. Wegh, H. Donker, A. Meijerink, R. Lamminmäki, and J. Hölsä, Phys. Rev. B **56**, 13841 (1997).
[36] M. Uhrmacher, K. Pampus, F. Bergmeister, D. Purschke, and K. Lieb, Nucl. Instrum. Methods Phys. Res. B **9**, 234 (1985).
[37] J. F. Ziegler, J. P. Biersack, and U. Littmark, *The Stopping and Range of Ions in Solids* (Pergamon, New York, 1999).
[38] C. Ronning, M. Dalmer, M. Uhrmacher, M. Restle, U. Vetter, L. Ziegeler, H. Hofsäss, T. Gehrke, K. Järrendahl, R. F. Davis, and the ISOLDE Collaboration, J. Appl. Phys. **87**, 2149 (2000).
[39] C. Sansonetti, M. Salit, and J. Reader, Appl. Opt. **35**, 74 (1996).
[40] J. Gruber, Spectral Measurements from the Arc Column of an Arc-Jet Wind Tunnel: Their Calibration and Analysis, NASA/AMES TR-721-06, Ames Research Center, Sunnyvale, CA, 1994.
[41] C. Morrison and R. Leavitt, in *Handbook on the Physics and Chemistry of Rare Earths*, edited by K. A. Gscheidner, Jr. and L. Eyring (North-Holland, Amsterdam, 1982), pp. 461–692.
[42] R. Wyckoff, *Crystal Structures* (Interscience, New York, 1965), Vol. 3.
[43] *International Tables for X-ray Crystallography*, edited by N. Henry and K. Lonsdale (Kynoch, Birmingham, 1969), Vol. 1.
[44] P. Vogl, J. Phys. C **11**, 251 (1978).
[45] S. Fraga, K. Saxena, and J. Karwowski, *Physical Science Data: 5*, *Handbook of Atomic Data* (Elsevier, Amsterdam, 1976).
[46] C. Morrison and R. Leavitt, J. Chem. Phys. **71**, 2366 (1979).
[47] C. Görller-Walrand and K. Binnemans, in *Handbook on the Physics and Chemistry of Rare Earths*, edited by K. A. Gscheidner, Jr. and L. Eyring (Elsevier Science B. V., Amsterdam, 1996), Vol. 23, pp. 121–283.
[48] W. Carnall, P. Fields, and K. Rajnak, J. Chem. Phys. **49**, 4412 (1968).
[49] J. Gruber, B. Zandi, and M. Reid, Phys. Rev. B **60**, 15643 (1999).
[50] J. Axe, Jr., J. Chem. Phys. **39**, 1154 (1963).
[51] W. Krupke and J. Gruber, Phys. Rev. **139**, A2008 (1965).
[52] D. Sardar, J. Gruber, B. Zandi, J. Hutchinson, and C. Trussell, J. Appl. Phys. **93**, 2041 (2003).
[53] J. Sytsma, G. Imbusch, and G. Blasse, J. Chem. Phys. **91**, 1456 (1983).